Design Heuristics and Optimization for Simple Adaptive Controllers With Applications to Spacecraft Proximity Operations

ANDRIY PREDMYRSKYY
STEVE ULRICH, Senior Member, IEEE
Carleton University, Ottawa, ON, Canada

Simple adaptive control manages unknown or time-varying systems with guaranteed performance by varying linear control gains until ideal system performance is achieved. The current work improves simple adaptive control designs through heuristics, optimization, and adaptive disturbance accommodation. Experimental results show that optimization successfully decreases the cost of designs and that adaptive disturbance compensation improves command tracking. Developed design heuristics expedite selection of simple adaptive control parameters. The developed design techniques improve confidence in implementations of simple adaptive controllers in physical systems while allowing designers to emphasize robustness, optimality, or disturbance rejection in their designs.

Manuscript received 25 March 2022; revised 20 August 2022; accepted 30 September 2022. Date of publication 5 October 2022; date of current version 9 June 2023.

DOI. No. 10.1109/TAES.2022.3211825

Refereeing of this contribution was handled by S. Sukumar.

This work was supported in part by the National Sciences and Engineering Research Council of Canada through an Alexander Graham Bell Canada Graduate Scholarship.

Authors' addresses: The authors are with the Department of Mechanical and Aerospace Engineering, Carleton University, Ottawa, ON K1S 5B6, Canada, E-mail: (andriypredmyrskyy@cmail.carleton.ca; steveulrich@cunet.carleton.ca). *(Corresponding author: Andriy Predmyrskyy.)*

I. INTRODUCTION

Recent increases in space activities throughout low-Earth orbit (LEO) have increased the rate of collisions, threatening *Kessler syndrome* [1]. Active deorbit techniques are the leading candidate for cleaning the LEO environment, which current models suggest requires the removal of at least five objects per year [2]. The only mission currently underway to manage LEO debris is Clearspace-1 from ESA [3] tasked with removing an object of known size and mass. Like deorbiting missions, in-orbit repair and sample-return missions have increased benefits under repeat operations, but must be completed under system uncertainty. A method for managing and improving autonomous spacecraft performance under uncertainty is invaluable to future successes in spacecraft operations.

Previous works have addressed various aspects of spacecraft control. Model predictive control leverages system models to optimize performance during flight [4], however higher uncertainty unavoidably contributes to system error. Di Mauro and Lavagna [5] provide a real-time nonlinear optimization technique through state-dependant Riccati equations that is computationally expensive. Sliding mode control has also been used to manage uncertainty in spacecraft [6].

Adaptive controllers offer a method of maintaining performance under uncertainty. Backstepping controllers have been proposed for spacecraft proximity operations [7] despite complex design and reliance on modeling. Of the adaptive control techniques that have been developed, simple adaptive control (SAC) [8] stands out as a computationally efficient algorithm with minimal complexity and impressive performance, which Ulrich et al. [10] have validated for use in spacecraft proximity operations.

The SAC architecture was developed in the 1980s as an evolution of model-reference adaptive controllers (MRACs) [11]. Barkana proved continuous time stability of the SAC equations for almost strictly positive real (ASPR) linear systems, and bounded stability of discrete ASPR systems [8]. The "feedforward parallelization" technique discovered by Barkana allows stabilizable linear systems to be augmented into linear ASPR systems [9].

Applications of SACs are numerous. Rusnak et al. [12] successfully applied SAC to a missile autopilot with classical inner-loop architecture to improve the performance. Ulrich and deLafontaine [13] showed that SAC excelled at controlling Mars atmospheric entry, even under the presence of large variations. Application of a differential evolution metaheuristic search was found to improve the cost of an SAC design by Takagi et al. [14], while Prabhakar et al. applied SAC to an UAV to show that SAC updates can be used to manage linear disturbances [15].

One notable drawback of SAC is the presence of "bursting" phenomena, where high-frequency oscillations occasionally appear without apparent provocation under inappropriate design parameter selection. No method of determining suitable design parameters currently exists.

In this context, the original contributions of this work are to improve the tools available to adaptive systems designers in order to simplify the design process, clarify the benefits and drawbacks of different techniques, and more generally improve confidence in adaptive control. Developed techniques are experimentally validated, a feature missing in previous works and critical to improving technical readiness. Specifically: heuristics are presented that aid in the preliminary design of SACs; nonlinear optimization techniques are tested in experiment and compared; and an implementation of adaptive disturbance compensation using the SAC update mechanism is extended to phase uncertainty and experimentally verified. Experiments are performed at Carleton University's Spacecraft Robotics and Control Laboratory (SRCL).

The rest of this article is organized as follows. The necessary background is summarized in Section II, while design techniques are developed and demonstrated in Section III. Design heuristics are applied to the motivating example in Section IV. Section V describes the experiments demonstrating heuristic design techniques, optimal design techniques, and adaptive disturbance compensation, the results of which are detailed in Section VI. Finally, Section VII concludes this article.

II. BACKGROUND

The basic SAC theory is described here for completeness. For a more detailed derivation of the theory, stability proof, and its linear disturbance compensation extension, the reader is referred to the work of Kaufman et al. [8], Barkana [9], and Prabhakar et al. [15].

A. SAC Formulation

The state-space model $\{\mathbf{A}_p, \mathbf{B}_p, \mathbf{C}_p, \mathbf{0}\}$ of the linear time-invariant (LTI) plant is represented by

$$\dot{\mathbf{x}}_p(t) = \mathbf{A}_p\mathbf{x}_p(t) + \mathbf{B}_p\mathbf{u}_p(t) \tag{1}$$

$$\mathbf{y}_p(t) = \mathbf{C}_p\mathbf{x}_p(t) \tag{2}$$

for plant order $n \in \mathbb{Z}^+$, inputs $m \in \mathbb{Z}^+$, and identical size of outputs m, to yield system matrices of sizes $\mathbf{A}_p \in \mathbb{R}^{n\times n}$, $\mathbf{B}_p \in \mathbb{R}^{n\times m}$, and $\mathbf{C}_p \in \mathbb{R}^{m\times n}$. A linear system $\{\mathbf{A}_m, \mathbf{B}_m, \mathbf{C}_m, \mathbf{0}\}$ is chosen by the designer for the adaptive controller to match, called the *ideal model*, given by the state-space system

$$\dot{\mathbf{x}}_m(t) = \mathbf{A}_m\mathbf{x}_m(t) + \mathbf{B}_m\mathbf{u}_c(t) \tag{3}$$

$$\mathbf{y}_m(t) = \mathbf{C}_m\mathbf{x}_m(t) \tag{4}$$

of model order $q \in \mathbb{Z}^+$ alongside input and output of sizes m. The signals for the ideal model are thus $\mathbf{x}_m \in \mathbb{R}^q$ states, $\mathbf{u}_m \in \mathbb{R}^m$ inputs, $\mathbf{y}_m \in \mathbb{R}^m$ outputs, as well as system matrices $\mathbf{A}_m \in \mathbb{R}^{q\times q}$, $\mathbf{B}_m \in \mathbb{R}^{q\times m}$, and $\mathbf{C}_m \in \mathbb{R}^{m\times q}$. The closed-loop system response will approach the ideal model, and thus, its selection directly affects the final system response, as well as steady-state gains and adaptation rate.

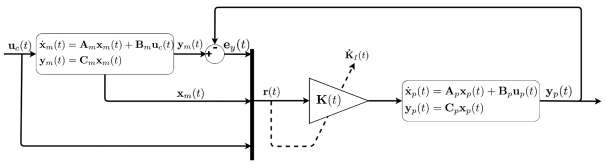

Fig. 1. SAC architecture.

The error between the real-system response and the ideal response is given by

$$\mathbf{e}_y(t) = \mathbf{y}_m(t) - \mathbf{y}_p(t) \tag{5}$$

called the *tracking error*. A new vector called the *reference signal* is constructed as follows:

$$\mathbf{r}(t) = \begin{bmatrix}\mathbf{e}_y^T(t) & \mathbf{x}_m^T(t) & \mathbf{u}_c^T(t)\end{bmatrix}^T. \tag{6}$$

The control $\mathbf{u}_p$ of an SAC is simply

$$\mathbf{u}_p(t) = \mathbf{K}(t)\mathbf{r}(t) \tag{7}$$

for time-varying gain $\mathbf{K}(t) \in \mathbb{R}^{p\times(2m+q)}$. The gain $\mathbf{K}(t)$ is further subdivided into a proportional part $\mathbf{K}_P(t) \in \mathbb{R}^{p\times(2m+q)}$ and integral part $\mathbf{K}_I(t) \in \mathbb{R}^{p\times(2m+q)}$ as follows:

$$\mathbf{K}(t) = \mathbf{K}_P(t) + \mathbf{K}_I(t). \tag{8}$$

The proportional gain adaptation is defined as

$$\mathbf{K}_P(t) = \mathbf{e}_y(t)\mathbf{r}^T(t)\boldsymbol{\Gamma}_P. \tag{9}$$

The design parameter $\boldsymbol{\Gamma}_P \in \mathbb{R}^{p\times(2m+q)}$, typically diagonal, reduces tracking error while adaptation of $\mathbf{K}_I(t)$ is still occurring but cannot alone converge to the ideal model. The resemblance between $\boldsymbol{\Gamma}_p$ and typical feedback control is discussed in Section III-H. The integral gain adaptation is

$$\dot{\mathbf{K}}_I(t) = \mathbf{e}_y(t)\mathbf{r}^T(t)\boldsymbol{\Gamma}_I - \mathbf{K}_I(t)\boldsymbol{\sigma} \tag{10}$$

with analogous design parameter $\boldsymbol{\Gamma}_I \in \mathbb{R}^{p\times(2m+q)}$, and new design parameter $\boldsymbol{\sigma} \in \mathbb{R}^{(2m+q)\times(2m+q)}$, called the *loss factor*. The design parameter $\boldsymbol{\Gamma}_I$ affects the rate of adaptation, and therefore, convergence to the ideal model. Meanwhile, the loss factor $\boldsymbol{\sigma}$ decays $\mathbf{K}(t)$ to avoid divergence in systems with noise. Given an initial gain $\mathbf{K}_0 \in \mathbb{R}^{m\times(2m+q)}$, (10) can be used to determine updates to the integral gain $\mathbf{K}_I(t)$. A diagram of the SAC architecture can be seen in Fig. 1.

B. SAC for Non-ASPR Systems

The SAC stability proof [9] applies for linear ASPR systems.

DEFINITION 1 (ASPR SYSTEM [9]) An LTI system $\{\mathbf{A}, \mathbf{B}, \mathbf{C}, \mathbf{D}\}$ is *almost strictly positive real* if by some constant feedback error gain the system becomes strictly positive real. That is to say that for $\widetilde{\mathbf{K}}_e \in \mathbb{R}^{m\times p}$, and transition matrix

$$\mathbf{A}_c = \mathbf{A} - \mathbf{B}\widetilde{\mathbf{K}}_e\mathbf{C} \tag{11}$$

then a second system $\{\mathbf{A}_c, \mathbf{B}, \mathbf{C}, \mathbf{D}\}$ is strictly positive real, satisfying the Kalman–Yakubovich–Popov conditions

$$\mathbf{P}\mathbf{A}_c + \mathbf{A}_c^T\mathbf{P} = -\mathbf{Q}, \qquad \mathbf{P}\mathbf{B} = \mathbf{C}^T \tag{12}$$

for some positive definite matrices $\mathbf{P} \in \mathbb{R}^{n\times n}$ and $\mathbf{Q} \in \mathbb{R}^{n\times n}$.

Few systems are ASPR, however, a technique called *feedforward parallelization* pioneered by Barkana [16] allows an augmented ASPR system to be constructed from any system that is stabilizable by a linear controller. Details on the construction of a feedforward parallelized system are found in Barkana [16]. Methods by Shibata et al. [17] and by Balas and Frost [18] also allow the construction of passive systems, however, only feedforward parallelization will be used here.

C. Model Matching Conditions

Matching conditions exist which, if met, allow a known plant to perfectly track a known ideal model.

THEOREM II.1 (MODEL MATCHING CONDITIONS [9]) For the plant $\{\mathbf{A}_p, \mathbf{B}_p, \mathbf{C}_p, \mathbf{0}\}$ and ideal model $\{\mathbf{A}_m, \mathbf{B}_m, \mathbf{C}_m, \mathbf{0}\}$, composite matrices $\mathbf{N}$ and $\mathbf{M}$ are constructed as follows:

$$\mathbf{M} = \begin{bmatrix} \mathbf{A}_p & \mathbf{B}_p \\ \mathbf{C}_p & \mathbf{0} \end{bmatrix},\ \mathbf{N} = \mathbf{M}^{-1} = \begin{bmatrix} \mathbf{N}_{11} & \mathbf{N}_{12} \\ \mathbf{N}_{21} & \mathbf{N}_{22} \end{bmatrix} \tag{13}$$

with $\mathbf{M}$ provably nonsingular for an ASPR system. Ideal model following occurs when the ideal model gains $\mathbf{K}_x^*$ and $\mathbf{K}_u^*$ satisfy the matching conditions

$$\mathbf{N}_{11}\mathbf{S}_{11} - \mathbf{S}_{11}\mathbf{A}_m^{-1} = -\mathbf{N}_{12}\mathbf{C}_m\mathbf{A}_m^{-1} \tag{14}$$

$$\mathbf{S}_{12} = \mathbf{N}_{11}\mathbf{S}_{11}\mathbf{B}_m \tag{15}$$

$$\mathbf{K}_x^* = \mathbf{N}_{21}\mathbf{S}_{11}\mathbf{A}_m + \mathbf{N}_{22}\mathbf{C}_m \tag{16}$$

$$\mathbf{K}_u^* = \mathbf{N}_{21}\mathbf{S}_{11}\mathbf{B}_m. \tag{17}$$

D. Disturbance Accommodation

The SAC adaptation mechanism can be used to eliminate a modeled linear disturbance [15]. A disturbance accommodating controller is described here and experimentally verified in Section V.

Assume that a disturbance $\mathbf{u}_d(t) \in \mathbb{R}^m$ can be modeled using a linear disturbance generator of the form

$$\dot{\mathbf{z}}_d(t) = \mathbf{F}_d\mathbf{z}_d(t) \tag{18}$$

$$\mathbf{u}_d(t) = \mathbf{\Theta}_d\mathbf{z}_d(t) \tag{19}$$

for model order $v \in \mathbb{Z}^+$, model states $\mathbf{z}_d \in \mathbb{R}^v$, update matrix $\mathbf{F}_d \in \mathbb{R}^{v\times v}$, and output transition $\mathbf{\Theta}_d \in \mathbb{R}^{m\times v}$. The similar estimated linear disturbance generator is denoted by a "$\hat{\ }$" symbol.

The adaptation for the disturbance accommodating gain follows from the previous adaptive gain formulations as

$$\mathbf{u}_z(t) = \mathbf{K}_z(t)\hat{\mathbf{z}}_d(t) = (\mathbf{K}_{zP}(t) + \mathbf{K}_{zI}(t))\hat{\mathbf{z}}_d(t) \tag{20}$$

$$\mathbf{K}_{zP}(t) = \mathbf{e}_y(t)\hat{\mathbf{z}}_d^T(t)\mathbf{\Gamma}_{zP} \tag{21}$$

$$\dot{\mathbf{K}}_{zI}(t) = \mathbf{e}_y(t)\hat{\mathbf{z}}_d^T(t)\mathbf{\Gamma}_{zI} - \mathbf{K}_{zI}(t)\boldsymbol{\sigma}_z \tag{22}$$

with $\mathbf{u}_z \in \mathbb{R}^m$ being the disturbance compensation, and $\mathbf{K}_z \in \mathbb{R}^{m\times v}$ the matrix of state gains. The design parameters $\mathbf{\Gamma}_{zP}$, $\mathbf{\Gamma}_{zI}$, and $\boldsymbol{\sigma}_z$ are analogous to their SAC counterparts, respectively, reducing tracking error during adaptation, increasing the adaptation rate, and decaying gains to avoid divergence in noisy systems. The reference signal can now be restated to include disturbance accommodation, and the design equations (7) to (10) resized to include the new signal.

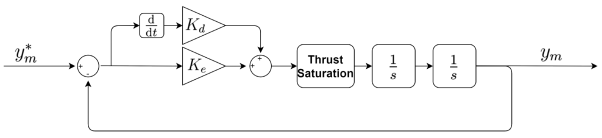

Fig. 2. Feasible model for thrust saturation, managed by a satisfying controller.

$$\mathbf{r}(t) = \begin{bmatrix} \mathbf{e}_y^T(t) & \mathbf{x}_m^T(t) & \mathbf{u}_m^T(t) & \hat{\mathbf{z}}_d^T(t) \end{bmatrix}^T. \tag{23}$$

III. SAC DESIGN METHODOLOGY AND HEURISTICS

In this section, SAC design parameters are presented and design heuristics are developed. First, the role of the ideal model is clarified. Heuristics for the integral adaptation, proportional adaptation, and loss factor are developed. Finally, optimization techniques are presented that are experimentally verified in Section V.

A. Ideal Model as Guidance

The SAC stability proof ensures that, when sufficient control power is present in an LTI ASPR system, the tracking error will go to zero and the system response will match the ideal model.

The model matching conditions clarify that only the form of the model determines if ideal gains exist. The only difference that ideal model selection has on an SAC response is to affect the magnitude of the converged gains, and in effect the final control output. For example, doubling the natural frequency of a second-order ideal model will double the ideal gains needed to achieve perfect following.

Physical systems are limited by their maximum control outputs, and thus, must take the maximum control activation into account. Ensuring control activations stay under a maximum is a fundamental guidance problem. The role of the ideal model should therefore be understood as affecting the guidance of the adaptive system.

B. Ideal Models for Nonlinear Systems; Feasible Models

The SAC equations assume that achieving a tracking error of zero is always possible. As such it is important that the model always represents an achievable response, even in the presence of nonlinearities. In this case, a *feasible model* can be constructed in the place of an ideal model, to ensure adaptation does not increase when the ideal model demands a physically impossible or nonlinear control activation $\mathbf{u}_p$.

In the case of a control saturation, for example, the ideal response may require more control authority than is available. The feasible model output replaces the ideal model output to ensure that no additional adaptation occurs due to otherwise unavoidable tracking error. However, the limiting nonlinearity must now be managed by a new *satisfying controller* to ensure the feasible model approaches the ideal model. An example of the new control problem

is shown in Fig. 2, where a satisfying controller has been added to the feasible model to ensure the feasible model output matches the ideal model output as often as possible. The concept of a feasible model can also be seen in Ulrich and deLafontaine [13] where guidance techniques are used to create a nonlinear ideal model.

C. ASPR Condition in Physical Systems

Theory suggests that no choice of proportional or integral adaptation is unstable for an LTI ASPR system [9]. However, any physical system will eventually fail to be accurately described by an ASPR plant, whether due to delay, noise, or instability at large gains. Instability in SAC for large adaptation parameters implies that the ASPR requirements are not met; designers must determine what constitutes stable parameter selection and choose adaptation parameters that keep the ASPR approximation applicable.

In this and the following subsections, an example system is used to demonstrate the effects of the SAC parameter selection. The plant

$$G(s) = \frac{1}{s+1} \tag{24}$$

is converted to a discrete state-space system with timestep 0.01 s. The ideal model

$$M(s) = \frac{1}{s^2+s+1} \tag{25}$$

is also converted to a discrete state-space model with the same timestep. The ideal gains for the SAC are

$$\mathbf{K}^* = \begin{bmatrix} K_e^* & K_{x1}^* & K_{x2}^* & K_u^* \end{bmatrix} = [0 \quad 1 \quad 1 \quad 0] \tag{26}$$

which is initialized with zero gains.

D. Linear Output and Maximum Acceptable Gains

When adaptation is omitted, the SAC output equation is linear

$$\mathbf{u}_c(t) = \mathbf{K}_e\mathbf{e}_y(t) + \mathbf{K}_x\mathbf{x}_m(t) + \mathbf{K}_u\mathbf{u}_m(t) = \mathbf{K}\mathbf{r}(t) \tag{27}$$

suggesting linear and nonlinear design tools can determine system performance for different gains. Call

$$\mathbf{K}_m = [\mathbf{K}_{\max,e}, \mathbf{K}_{\max,x}, \mathbf{K}_{\max,u}] \tag{28}$$

the matrix of maximum acceptable gains for (27), the values of which are chosen by the designer through experiment, analysis, or from requirements. The choice of these maximum values is a design decision and will vary with the system in consideration.

The example system is continuous-time ASPR, however analysis reveals the discrete system is unstable for feedback gains above 200 and as such *cannot* be ASPR. The maximum feedback gain in the example is a limitation that proper parameter selection will avoid. The maximum allowable SAC gains for the example system are chosen to be

$$\mathbf{K}_m = [150, 10, 10, 1]. \tag{29}$$

E. Integral Adaptation Parameter Selection

The integral of the tracking error with the reference signal is abbreviated as

$$\mathbf{K}_F(t) = \int_0^t \mathbf{e}_y(\tau)\mathbf{r}^T(\tau)\mathrm{d}\tau = \int_0^t \mathbf{I}_K(\tau)\mathrm{d}\tau \tag{30}$$

where $\mathbf{K}_F$ is called the *forcing gain*, and $\mathbf{I}_K$ the *gain impulse*.

If either $\mathbf{K}_F$ or $\mathbf{I}_k$ can be determined, then the remaining equation for the maximum acceptable adaptation parameter becomes

$$\mathbf{K}_m \geq \mathbf{K}_F(t)\mathbf{\Gamma}_I + \mathbf{K}_0. \tag{31}$$

At equality, (31) is a matrix equation for $\mathbf{\Gamma}_I$, which can always be solved in the SISO case. The adaptation parameter estimate found through (31) is called $\hat{\mathbf{\Gamma}}_I \in \mathbb{R}^{(2m+q)\times(2m+q)}$.

F. Gain Impulse Estimation

To ensure $\mathbf{K}_m$ is not exceeded, an estimate of the forcing gain must be found, which is less than the real forcing gain. The forcing gain estimate is defined to be

$$\hat{\mathbf{K}}_F(t) = \int_0^t |\hat{\mathbf{e}}_y(\tau)|\,|\hat{\mathbf{r}}^T(\tau)|\mathrm{d}\tau \geq \int_0^t \mathbf{e}_y(\tau)\,\mathbf{r}^T(\tau)\mathrm{d}\tau \tag{32}$$

for estimated tracking error $\hat{\mathbf{e}}_y$ and reference signal $\hat{\mathbf{r}}$. Three estimates are compared here.

1) *Uninformed Estimate:* The worst-case system response is assumed over the course of a representative scenario to determine the worst case adaptation parameters. The example system under only step commands has maximum values of

$$\begin{aligned} \hat{\mathbf{e}}_y &= \max(|\mathbf{e}_y(t)|) = |u_c| = 1 \\ \hat{\mathbf{r}} &= \max\left(\begin{bmatrix} |\mathbf{e}_y^T(t)| & |\mathbf{x}_m^T(t)| & |\mathbf{u}_m^T(t)| \end{bmatrix}^T\right) \\ &= [1 \quad 0.37 \quad 1 \quad 1]^T. \end{aligned}$$

The bounded forcing gain estimate is, therefore,

$$\hat{\mathbf{K}}_F = \int_0^t |\hat{\mathbf{e}}_y(\tau)|\,|\hat{\mathbf{r}}^T(\tau)|\mathrm{d}\tau = t\hat{\mathbf{e}}_y\hat{\mathbf{r}}^T \tag{33}$$

which, when used with (31) yields

$$\hat{\mathbf{\Gamma}}_I = \mathrm{diag}\left([1.59390 \quad 0.0295 \quad 0.0797 \quad 0.008]\right). \tag{34}$$

The system response for this parameter estimate is shown in Fig. 3.

2) *Maximum Value Estimate:* Call $\mathbf{e}_y(t, \mathbf{\Gamma}_I)$ the tracking error during a simulated response for an SAC using parameters $\mathbf{\Gamma}_I$, and $\mathbf{r}(t, \mathbf{\Gamma}_I)$ the reference signal under the same parameters. An estimate for the new maximum signals can be found as

$$\hat{\mathbf{e}}_y(\mathbf{\Gamma}_I) = \max(|\mathbf{e}_y(t, \mathbf{\Gamma}_I)|) \tag{35}$$

$$\hat{\mathbf{r}}(\mathbf{\Gamma}_I) = \max\left(\begin{bmatrix} |\mathbf{e}_y(t, \mathbf{\Gamma}_I)| & |\mathbf{x}_m(t, \mathbf{\Gamma}_I)| & |\mathbf{u}_m(t, \mathbf{\Gamma}_I)| \end{bmatrix}^T\right) \tag{36}$$

which yields a new forcing gain $\hat{\mathbf{K}}_F$ through

$$\hat{\mathbf{K}}_F = t\hat{\mathbf{e}}(\mathbf{\Gamma}_I)\hat{\mathbf{r}}^T(\mathbf{\Gamma}_I). \tag{37}$$

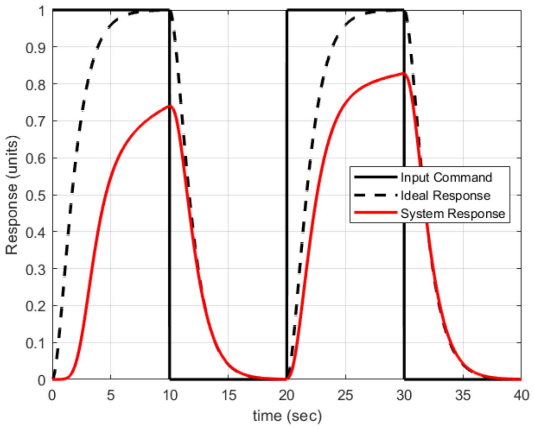

Fig. 3. Uninformed estimate response.

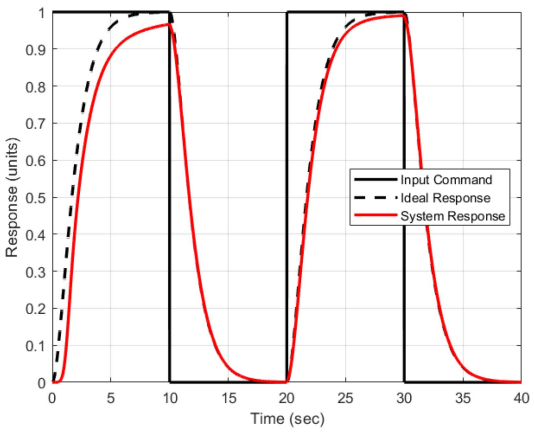

Fig. 4. Maximum value estimate response.

A simulation can be run with the new SAC parameters, and the estimate repeated until satisfactory convergence in the forcing gain has been achieved.

Stability of the maximum value estimate over successive simulations and re-evaluations of $\hat{\mathbf{K}}_F$ is likely, and difficult to prove without further research on the time response of a system under SAC.

The final adaptation parameter estimate for the example system is found to be

$$\hat{\mathbf{\Gamma}}_I = \text{diag}\left(\begin{bmatrix} 66.1 & 2.85 & 1.05 & 0.105 \end{bmatrix}\right). \tag{38}$$

The controller determined by the maximum value estimate is shown in Fig. 4.

3) *Simulated Forcing Gain:* The forcing gain can also be estimated from simulation by direct evaluation of

$$\hat{\mathbf{K}}_F = \int_0^t |\mathbf{e}_y(\tau, \mathbf{\Gamma}_I)|\,|\mathbf{r}^T(\tau, \mathbf{\Gamma}_I)|\mathrm{d}\tau. \tag{39}$$

The gain impulse estimate is then used to find a new set of adaptation parameters through (31). This process can then be iterated.

The adaptation parameters estimated directly from simulation of the example system are

$$\hat{\mathbf{\Gamma}}_I = \text{diag}\left(\begin{bmatrix} 2.1 \times 10^7 & 1.7 \times 10^4 & 5.3 \times 10^3 & 325 \end{bmatrix}\right). \tag{40}$$

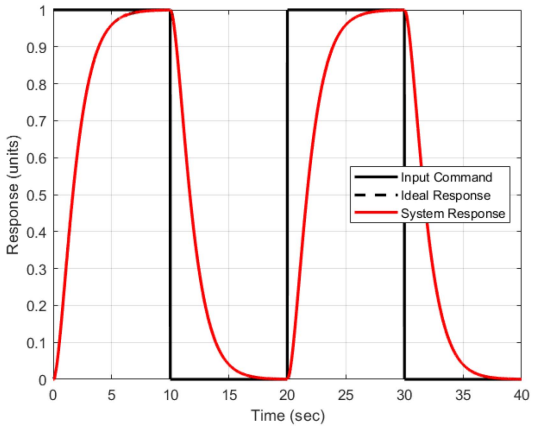

Fig. 5. Simulated forcing gain estimate response.

Fig. 5 shows the final system response, where the signals for the ideal model output and the system response overlap.

G. Steady State Gains Under Noise and Signal Covariance

The loss factor can be included in the gain update from (31) to yield a new set of conditions

$$\mathbf{K}_m \geq \int_0^t \left(\mathbf{e}_y(\tau)\mathbf{r}^T(\tau)\mathbf{\Gamma}_I - \mathbf{K}_l(\tau)\boldsymbol{\sigma}\right)\mathrm{d}\tau + \mathbf{K}_0. \tag{41}$$

The integral in (41) is zero at the maximum gain when

$$\hat{\mathbf{I}}_K\mathbf{\Gamma}_I = \mathbf{K}_m\boldsymbol{\sigma}. \tag{42}$$

Setting the integral in (41) to zero and solving over Δt also gives an equation for $\boldsymbol{\sigma}$ as

$$\hat{\mathbf{K}}_F\mathbf{\Gamma}_I = \Delta t\mathbf{K}_0\boldsymbol{\sigma}. \tag{43}$$

The aforementioned equation implies that knowledge of the system noise can be leveraged by the designer to specify a steady-state value for the tracking error gain, called $\mathbf{K}_{\text{ss}}$, through the use of the loss factor.

Consider that the measured signal $\mathbf{y}_p$ includes uncorrelated gaussian zero-mean noise with variance

$$\text{Var}(\mathbf{y}_p) = \mathbf{E}\left[(\mathbf{y}_p - \mathbf{y}_{\text{avg}})^2\right] = \boldsymbol{\delta}^2. \tag{44}$$

Assuming either a steady-state system or a converged and zero error system, setting (10) to zero yields the design equation

$$\mathbf{K}_{ss}\hat{\boldsymbol{\sigma}} = \boldsymbol{\delta}^2\mathbf{\Gamma}_I \tag{45}$$

which can be solved for $\hat{\boldsymbol{\sigma}}$.

The noise of variance $\delta = 1$ was applied to the example system, and the effects were observed. For a desired steady-state feedback gain of $\mathbf{K}_{\text{ss}} = 5$ under adaptation parameters

$$\mathbf{\Gamma}_I = \text{diag}\left([1.5939 \quad 0.0295 \quad 0.0797 \quad 0.008]\right) \tag{46}$$

evaluating (45) results in a value of $\sigma_e = 0.2391$. The resultant gain response under noise is demonstrated in Fig. 6.

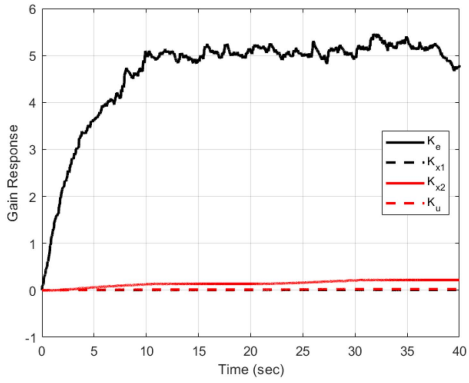

Fig. 6. Gains under noise and appropriate $\boldsymbol{\sigma}$ selection.

H. Proportional Adaptation as Quadratic Control

An SAC with only proportional adaptations has output

$$\mathbf{u}_p(t) = \mathbf{e}_y(t)\mathbf{r}^T(t)\boldsymbol{\Gamma}_P\mathbf{r}(t) \tag{47}$$

which resembles a negative feedback controller with adaptive gain $\mathbf{r}^T\boldsymbol{\Gamma}_P\mathbf{r}$. Selection of the proportional adaptation parameter corresponds to solutions of

$$\mathbf{u}_{p,b} = \mathbf{e}_{y,b}\mathbf{r}_b^T\boldsymbol{\Gamma}_P\mathbf{r}_b \tag{48}$$

such that $\mathbf{r}_b$ and $\mathbf{e}_{y,b}$ are the reference signal and tracking error at which a given control input $\mathbf{u}_{p,b}$ occurs.

The example system is given poorly chosen adaptations of

$$\boldsymbol{\Gamma}_I = \mathrm{diag}\left([10 \quad 1000 \quad 1000 \quad 0]\right) \tag{49}$$

with no loss $\boldsymbol{\sigma}$ or proportional control $\boldsymbol{\Gamma}_P$. The results of the controller are seen in Fig. 7(a), where significant bursting is present. The magnitude of the bursts can be decreased by direct application of (48). Boundary conditions of

$$\mathbf{e}_{y,b} = 0.1,\ \mathbf{u}_{p,b} = 3,\ \mathbf{r}_b = [\mathbf{e}_{y,b} \quad 0 \quad 0 \quad 0]^T \tag{50}$$

yield a proportional adaptation of $\Gamma_{eP} = 3000$ whose application results in Fig. 7(b).

I. Phase Uncertainty in SAC Disturbance Compensation

Previous results in adaptive disturbance compensation [15] can be easily extended to phase uncertainty. The solutions of the linear disturbance model provided in (18) and (19) must be either exponential or sinusoidal. A sinusoid can be described through

$$\sin(\omega t + \phi) = a\sin(\omega t) + b\cos(\omega t) \tag{51}$$

for the angular frequency $\omega \in \mathbb{R}$ in rad/s, phase shift $\phi \in \mathbb{R}$ in rad, and superposition magnitudes $a, b \in \mathbb{R}$. Therefore, phase uncertainty in the disturbance compensation can be addressed by increasing the order of the disturbance compensation model.

J. SAC Optimization and Parameter Search

Work by Takagi et al. [14], and subsequent development by Predmyrskyy and Ulrich [21] for spacecraft proximity operations determined that metaheuristic searches

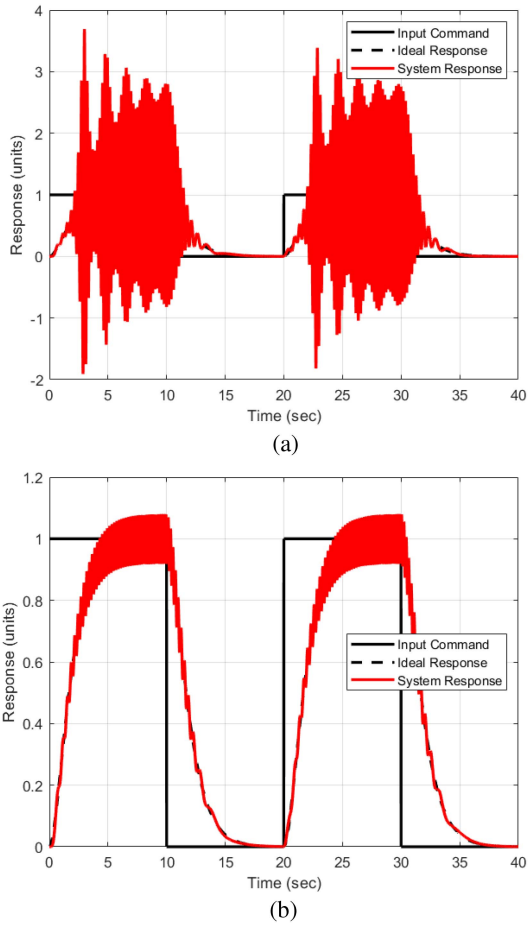

Fig. 7. Poorly tuned system with and without proportional adaptation. (a) Without proportional adaptation. (b) With boundary heuristic proportional adaptation.

are effective at lowering the linear quadratic cost of an SAC design. An attempt is made to determine if nonlinear optimization techniques are comparable to metaheuristic searches for SAC optimization through experimental verification in Section V, the equations for which are developed here.

In both nonlinear and metaheuristic optimizations, the cost function to be minimized is

$$O(t) = \int_0^t \mathbf{e}_y^T(\tau)\mathcal{Q}\mathbf{e}_y(\tau) + \mathbf{u}_p^T(\tau)\mathcal{R}\mathbf{u}_p(\tau)d\tau \tag{52}$$

for the weighing matrices $\mathcal{Q} \in \mathbb{R}^{m\times m}$ and $\mathcal{R} \in \mathbb{R}^{m\times m}$.

1) *Nonlinear Optimization:* The SAC design equations are implemented and optimized using the sequential quadratic programming (SQP) method outlined in Schittkowski [22] through MATLAB's `fmincon` routine.

A linear model approximation of the experimental system response is used during optimization, augmented through feedforward parallelization by a stabilizing controller. A proportional-derivative (PD) controller with proportional gain $K_p = 0.1$ and derivative gain $K_d = 1$ stabilizes the system. The continuous time system is

characterized by $\{\mathbf{A}_{\text{SPOT}}, \mathbf{B}_{\text{SPOT}}, \mathbf{C}_{\text{SPOT}}, \mathbf{D}_{\text{SPOT}}\}$ with

$$\mathbf{A}_{\text{SPOT}} = \begin{bmatrix} -1 & 0 & 0 \\ 1 & 0 & 0 \\ 0 & 1 & 0 \end{bmatrix}, \ \mathbf{B}_{\text{SPOT}} = \begin{bmatrix} 1 \\ 0 \\ 0 \end{bmatrix} \tag{53}$$

$$\mathbf{C}_{\text{SPOT}} = [0.1 \quad 0.059 \quad 0.0059], \ \mathbf{D}_{\text{SPOT}} = [0] \tag{54}$$

and converted to an equivalent discrete system at 10 Hz, called $\{\mathbf{A}_{\text{SPOT}d}, \mathbf{B}_{\text{SPOT}d}, \mathbf{C}_{\text{SPOT}d}, \mathbf{D}_{\text{SPOT}d}\}$

Gain adaptations are constructed through Euler integration of the nonlinear update equations, as in Liu and Lu [23]. For timestep $k \in \mathbb{Z}^+$, the discrete plant update equations are given in (56). The equality constraint for the gain updates is given by (57), while the controller outputs are given by (58). The remaining SAC design equations are implemented as equality constraints across each of the timesteps k, given by (60)–(62).

The ideal model outputs and states are precomputed for a second-order ideal model of natural frequency $\omega_n = 3.33$ rad/s and damping coefficient $\zeta = 0.6$. The ideal model signals are called $y_m \in \mathbb{R}$ for the output, $\mathbf{x}_m \in \mathbb{R}^2$ for the model states, and $u_c \in \mathbb{R}$ for the model inputs.

The final nonlinear optimization problem is written as

$$\underset{\mathbf{x}\in\mathcal{V}}{\text{minimize}} \quad O = \int_0^{t_f} \mathbf{e}_y^T(k)\mathcal{Q}\mathbf{e}_y(k) + u_p^T(k)\mathcal{R}u_p(k)\mathrm{d}k \tag{55}$$

$$\begin{aligned} \underset{k=1,\ldots,t_f}{\text{subject to}} \quad & \left(\mathbf{I}_3 - \frac{h}{2}\mathbf{A}_{\text{SPOT}d}(k)\right)\mathbf{x}(k) \\ & = \left(\mathbf{I}_3 + \frac{h}{2}\mathbf{A}_{\text{SPOT}d}(k-1)\right)\mathbf{x}(k-1) \\ & \quad + \frac{h}{2}\mathbf{B}_{\text{SPOT}d}\left(\mathbf{u}_p(k) + \mathbf{u}_p(k-1)\right) \end{aligned} \tag{56}$$

$$\begin{aligned} \mathbf{K}_I(k) &= \mathbf{K}_I(k-1) \\ &\quad + \frac{h}{2}\mathbf{e}_y(k)\mathbf{r}^T(k)\mathbf{\Gamma}_I \\ &\quad + \frac{h}{2}\mathbf{e}_y(k-1)\mathbf{r}^T(k-1)\mathbf{\Gamma}_I \end{aligned} \tag{57}$$

$$\mathbf{u}_p(k) = \mathbf{e}_y(k)\mathbf{r}^T(k)\mathbf{\Gamma}_P\mathbf{r}(k) + \mathbf{K}_I(k)\mathbf{r}(k) \tag{58}$$

$$\mathbf{r}(k) = \begin{bmatrix} y_m(k) - y_p(k) & \mathbf{x}_m(k) & u_c(k) \end{bmatrix}^T \tag{59}$$

$$\mathbf{u}_p(k) = \mathbf{K}(k)\mathbf{r}(k) \tag{60}$$

$$\mathbf{K}(k) = \mathbf{K}_P(k) + \mathbf{K}_I(k) \tag{61}$$

$$\mathbf{K}_P(k) = \mathbf{e}_y(k)\mathbf{r}^T(k)\mathbf{\Gamma}_P \tag{62}$$

where t_f is the final iteration, $\mathbf{x}$ the system states, and $\mathcal{V}$ the set of allowable states. Nonlinear SQP optimized an SAC design for a step input of 1 m over a command time of 100 s under the given optimization problem and zero initial parameters. The output controller determined by nonlinear optimization is summarized in Table I.

2) *Metaheuristic Optimization for SAC Design:* An overview of metaheuristic algorithms is available in Wahab et al. [19], from which strategy-adaptive differential evolution (SaDE) and selection particle swarm optimization (SPSO) are selected to optimize SAC designs. The reader is referred to Predmyrskyy and Ulrich [21] for an outline of the metaheuristic algorithms used.

TABLE I
Experimental and Optimized SAC Parameters

Parameter	Manually designed using heuristics	Nonlinearly optimized	SaDE optimized	SPSO optimized	Disturbance without compensation	Disturbance with compensation
Γ_{eP}	200	2.8	0	0	0	0
Γ_{x_1P}	0	1.8×10^{-5}	0	0	0	0
Γ_{x_2P}	0	0.8120	0	0	0	0
Γ_{uP}	0	3.25	0	0	0	0
Γ_{eI}	5.64×10^4	6.63	7.04×10^3	1×10^4	1×10^4	1×10^4
Γ_{x_1I}	6.66	4.77×10^{-5}	0	0	0.1	0.1
Γ_{x_2I}	679.9	160	4.43×10^3	183.0	0.1	0.1
Γ_{uI}	6.66	2.63×10^{-4}	9.18	0	0.01	0.01
Γ_{zI}	0	0	0	0	0	1
σ	0.0011	0	0	0.02	0	0

A nonlinear simulation of the experimental environment was used alongside SaDE and SPSO searches to determine optimal controller designs. The results of both the SaDE and SPSO search are outlined in Table I.

IV. MOTIVATING EXAMPLE

The SAC design techniques developed in Section III are implemented in experiment as trajectory control for the SRCL's three degree of freedom spacecraft proximity operations testbed (SPOT), which will serve as a motivating example.

The augmented plant dynamics match those given by $\{\mathbf{A}_{\text{SPOT}}, \mathbf{B}_{\text{SPOT}}, \mathbf{C}_{\text{SPOT}}, \mathbf{D}_{\text{SPOT}}\}$, which meets the ASPR requirements. The ideal model is similarly a second-order system of natural frequency $\omega_n = 3.33$ rad/s and damping coefficient $\zeta = 0.6$.

The set of maximum allowable gains for the system is chosen to be

$$\mathbf{K}_m = [100 \quad 7.29 \quad 10.82 \quad 7.29] \tag{63}$$

which is a set of stable and well performing linear SISO gains for the system.

Design heuristics are used to determine appropriate selections of the adaptation parameters. The forcing gain is determined for a reference circular trajectory and used to solve (31). After 30 iterations of parameter estimation and simulation, the final integral adaptation parameters for the SISO system are found to be

$$\mathbf{\Gamma}_I = \text{diag}\left(\begin{bmatrix} 5.64 \times 10^4 & 6.66 & 679.9 & 6.66 \end{bmatrix}\right). \tag{64}$$

The proportional adaptation design heuristic is applied to ensure that at a distance of 0.1 m, the controller will always apply at least half the maximum thrust of 0.4 N. Solving (48) for $\mathbf{\Gamma}_P$ and boundary values of

$$e_{y,b} = 0.1, u_{p,b} = 0.2, r_b^T = [0.1 \quad 0 \quad 0 \quad 0] \tag{65}$$

yields a proportional adaptation matrix of

$$\mathbf{\Gamma}_P = \text{diag}\left([200 \quad 0 \quad 0 \quad 0]\right). \tag{66}$$

Finally, the loss factor is chosen to meet the designed maximum steady-state feedback gain of 100. Since the position noise variation is known to be $\delta^2 = 1 \times 10^{-7}\text{m}^2$, (45) can be used alongside the designed integral adaptation parameter to determine a loss factor of $\sigma = 0.0011$.

V. EXPERIMENTAL VALIDATION

Nonlinearly optimized, metaheuristic optimized, and heuristic designed SACs are implemented for the position control of a spacecraft in Carleton's SRCL and compared. The performance of SAC under disturbance is also compared with and without adaptive disturbance compensation when the frequency of the disturbance is known but the amplitude and phase are unknown.

A. SAC Positional Tracking Experimental Setup and Controller Development

Previous work by Ulrich et al. [20] has determined that SAC can be implemented to successfully control the position of a spacecraft during spacecraft proximity operations under significant mass uncertainty. Current position tracking experiments will clarify the applicability of the various design techniques outlined in Section III to a practical control scenario.

Only position dynamics are considered, and as such the system dynamics are described by the double-integrator form

$$F_x = ma_x = m\ddot{x},\ F_y = ma_y = m\ddot{y} \tag{67}$$

where $F_x \in \mathbb{R}$ and $F_y \in \mathbb{R}$ denote the applied force in the x- and y-directions, respectively, alongside mass $m \in \mathbb{R}$ and positions in the x- and y-directions of $x \in \mathbb{R}$ and $y \in \mathbb{R}$.

The weighing matrices $\mathcal{Q}$ and $\mathcal{R}$ used are

$$\mathcal{Q} = \begin{bmatrix} 1 & 0 \\ 0 & 1 \end{bmatrix},\ \mathcal{R} = \begin{bmatrix} 10 & 0 \\ 0 & 10 \end{bmatrix}. \tag{68}$$

For the adaptive controller, feedforward parallelization is added to the system to create an ASPR augmented plant. The inverse of this stabilizing controller is found and used to create an augmented plant following

$$\mathbf{y}_a(s) = \mathbf{y}_p(s) + \mathbf{u}_p(s)\mathbf{I}_2 \frac{1}{1\,s + 0.1} \tag{69}$$

alongside a second-order ideal model of natural frequency $\omega_n = 3.33$ rad/s and damping coefficient $\zeta = 0.6$.

The SAC design parameters are encoded as

$$\mathbf{\Gamma}_P = \text{diag}\left(\begin{bmatrix} \Gamma_{eP}\mathbf{I}_2 & \Gamma_{x_1P}\mathbf{I}_2 & \Gamma_{x_2P}\mathbf{I}_2 & \Gamma_{uP}\mathbf{I}_2 \end{bmatrix}\right) \tag{70}$$

$$\mathbf{\Gamma}_I = \text{diag}\left(\begin{bmatrix} \Gamma_{eI}\mathbf{I}_2 & \Gamma_{x_1I}\mathbf{I}_2 & \Gamma_{x_2I}\mathbf{I}_2 & \Gamma_{uI}\mathbf{I}_2 \end{bmatrix}\right) \tag{71}$$

$$\boldsymbol{\sigma} = \text{diag}\left([\sigma\mathbf{I}_2 \quad \mathbf{0} \quad \mathbf{0} \quad \mathbf{0}]\right) \tag{72}$$

and the specific values used for each parameter are outlined in Table I.

A feasible model is developed from the ideal model and the maximum platform thrust of 0.4 N. The satisfying controller used in the feasible model is a PD controller with proportional gain of $\mathbf{K}_{p,\text{sat}} = 3.16$ and derivative gain $\mathbf{K}_{d,\text{sat}} = 10.0$. The system begins with zero initial gains.

The heuristic design found in Section IV is implemented and compared to SQP optimization, SaDE optimization, and SPSO optimization. Optimizations are performed through nonlinear and metaheuristic searches described in Section III under the cost function (52), starting from a design of all zero parameters. The nonlinear optimization is conducted using the optimization problem presented in (55)–(62). Metaheuristic searches are conducted on a circular test trajectory with angular velocity 0.03 rad/s and radius 1 m. Metaheuristic searches for SAC design parameters are done using calls to the accurate and nonlinear SPOT simulation directly, thereby incorporating any nonlinearities and system behaviors into the search. The design parameters determined by each of the four methods are shown in Table I.

The experimental test trajectory is governed by the equations

$$x_{\text{cmd}}(t) = 0.5\cos(0.03t) + 0.35\sin(3 \cdot 0.03t) \tag{73}$$

$$y_{\text{cmd}}(t) = 0.5\sin(0.03t) + 0.35\cos(3 \cdot 0.03t). \tag{74}$$

Experiments are conducted to determine the trajectory tracking performance of each of the manually designed SAC, nonlinearly optimized SAC, SaDE optimized SAC, and SPSO optimized SAC in Section VI. Each controller is commanded to follow the experimental trajectory for 200 ss, and the test is repeated ten times. All adaptive controllers begin with zero initial gains.

B. SAC Disturbance Compensation Experimental Setup

The disturbance accommodating controller developed in Section III is experimentally validated using a virtual linear disturbance. Tests are performed for two controllers: one controller with manually chosen SAC parameters, without disturbance compensation, and under virtual linear disturbance; and an identical controller with additional adaptive disturbance compensation. The disturbance compensation follows the linear disturbance generator and model described in Section III, where the frequency of the disturbances, but not the phase or amplitude, are known. A virtual disturbance is created by including an unknown force command to the thruster output. The new form of the design parameters is

$$\mathbf{\Gamma}_P = \text{diag}\left(\begin{bmatrix} \Gamma_{eP}\mathbf{I}_2 & \Gamma_{x_1P}\mathbf{I}_2 & \Gamma_{x_2P}\mathbf{I}_2 & \Gamma_{uP}\mathbf{I}_2 & \Gamma_{zP}\mathbf{I}_2 \end{bmatrix}\right) \tag{75}$$

$$\mathbf{\Gamma}_I = \text{diag}\left(\begin{bmatrix} \Gamma_{eI}\mathbf{I}_2 & \Gamma_{x_1I}\mathbf{I}_2 & \Gamma_{x_2I}\mathbf{I}_2 & \Gamma_{uI}\mathbf{I}_2 & \Gamma_{zI}\mathbf{I}_4 \end{bmatrix}\right) \tag{76}$$

$$\boldsymbol{\sigma} = \text{diag}\left([\sigma\mathbf{I}_2 \quad \mathbf{0} \quad \mathbf{0} \quad \mathbf{0} \quad \mathbf{0}]\right). \tag{77}$$

The SAC design parameters with and without disturbance accommodation are outline in Table I. Disturbances are provided by the signals

$$\mathbf{u}_d(t) = \begin{bmatrix} 0.2\sin(0.03t + 2.06) \\ 0.1\sin(0.06t + 5.87) \end{bmatrix} \tag{78}$$

The SAC disturbance accommodation uses the linear disturbance model

$$\hat{\mathbf{z}}_d(t) = [\sin(0.03t) \quad \cos(0.03t) \quad \sin(0.06t) \quad \cos(0.06t)]^T. \tag{79}$$

Both the compensated and uncompensated controllers are made to track the two-frequency cycloid used in the SAC positional tracking experiment described in Section V-A under the virtual disturbance. Ten experiments are performed for both the uncompensated and compensated cases .

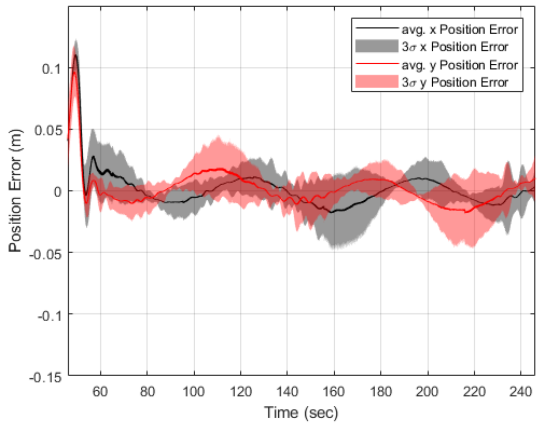

Fig. 8. Heuristic designed controller position error to the command, with 3σ standard deviation.

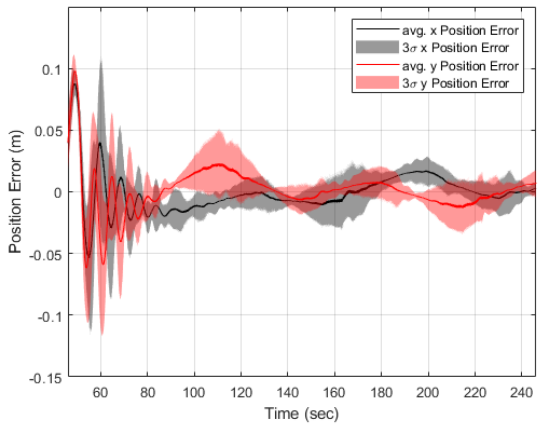

Fig. 9. Nonlinearly optimized controller position error to the command, with 3σ standard deviation.

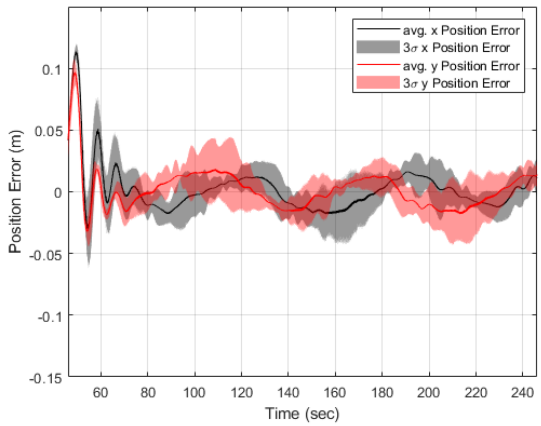

Fig. 10. SaDE optimized controller position error to the command, with 3σ standard deviation.

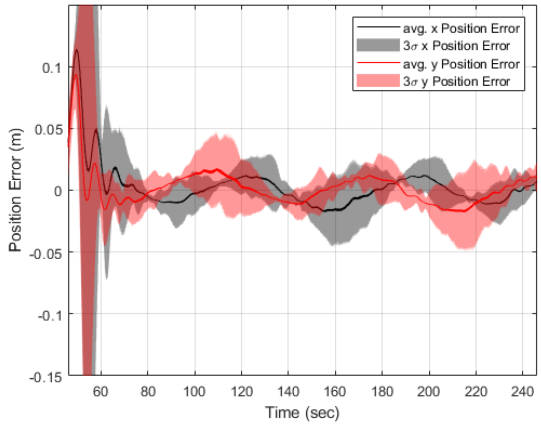

Fig. 11. SPSO optimized controller position error to the command, with 3σ standard deviation.

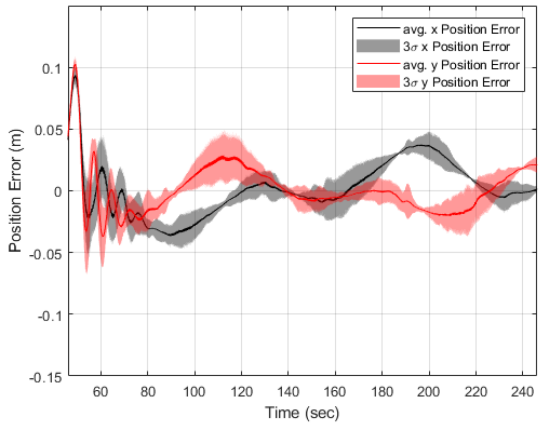

Fig. 12. SAC position error, with 3σ standard deviation under linear disturbance without compensation.

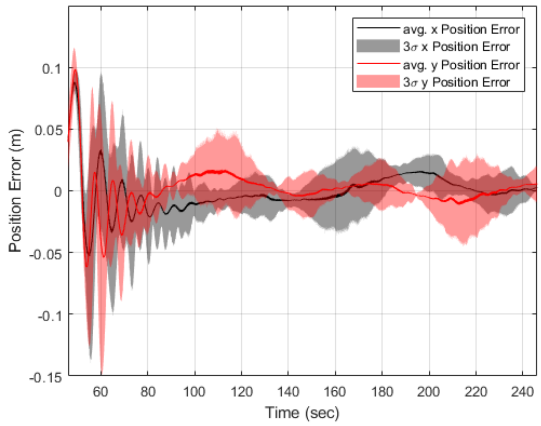

Fig. 13. SAC position error, with 3σ standard deviation under linear disturbance with compensation.

VI. EXPERIMENTAL RESULTS

The trajectory tracking experiment was performed, and the error to the command of each system is demonstrated in Figs. 8–11. The linear quadratic cost of the average run for each controller is compiled in Table II. The disturbance compensation experiment was performed, and the

TABLE II
Experimental Linear-Quadratic Cost of SAC Designs

	Heuristic designed	Nonlinearly optimized	SaDE optimized	SPSO optimized
Cost	29.60	41.11	27.07	19.94

error to the command of the SAC with and without disturbance compensation is demonstrated in Figs. 12 and 13, respectively.

The heuristic designed SAC converges quickly on the ideal model, and converged the fastest of the surveyed controllers. Nonlinear optimization is not able to determine SAC parameters that perform well compared to other controller designs in experiment. Both the SaDE and SPSO optimizations lowered the cost compared to the heuristic design through smaller control activations.

Fig. 12 includes the additional position error, caused by the virtual disturbance, which is noticeably reduced in Fig. 13. Notably, the convergence time has increased under compensation.

VII. CONCLUSION

The need to increase spacecraft autonomy can be felt in many sectors, including in-flight repair, sample return missions, and active debris deorbiting. SAC offers an uncomplicated method of improving the spacecraft autonomy.

This work has presented and validated design methodologies for the implementation of simple adaptive controllers. The selection of the ideal model is reinterpreted as a guidance problem, and the feasible model concept defined. Heuristics were presented for the selection of controller parameters. The effects of optimization on the design of simple adaptive was shown. Adaptive linear disturbance accommodation was experimentally shown to compensate for disturbances of known frequency, but unknown phase and magnitude.

Future work on simple adaptive controllers may focus on the role of augmentation in the SAC response. Convergence conditions for the presented disturbance accommodation scheme should be investigated.

REFERENCES

[1] J. N. Pelton, "Introduction," in *New Solutions for the Space Debris Problem*, 1st ed. New York, NY, USA: Springer, 2015, ch. 1, sec. 1, pp. 1–10.

[2] J. C. Liou and N. L. Johnson, "A sensitivity study of the effectiveness of active debris removal in LEO," *Acta Astronautica*, vol. 64, no. 2–3, pp. 236–243, 2009.

[3] M. Juillard, M. Richard-Noca, and J.-P. Kneib, "Dedicated on-board computer for active debris removal mission," in *Proc. 34th Small Satell. Conf.*, 2020.

[4] M. Leomanni, E. Rogers, and S. B. Gabriel, "Explicit model predictive control approach for low-thrust spacecraft proximity operations," *J. Guid., Control, Dyn.*, vol. 37, no. 6, pp. 1780–1790, 2014, doi: 10.2514/1.G000477.

[5] G. Di Mauro, M. Schlotterer, S. Theil, and M. Lavagna, "Nonlinear control for proximity operations based on differential algebra," *J. Guid., Control, Dyn.*, vol. 38, no. 11, pp 2173–2187, 2015, doi: 10.2514/1.G000842.

[6] K. Zhang, G. Duan, and M. Ma, "Adaptive sliding-mode control for spacecraft relative position tracking with maneuvering target," *Int. J. Robust Nonlinear Control*, vol. 28, pp. 5786–5810, 2018, doi: 10.1002/mc.4346.

[7] L. Sun and W. Huo, "Robust adaptive backstepping control for autonomous spacecraft proximity maneuvers," *Int. J. Control, Automat., Syst.*, vol. 14, no. 3, pp. 753–762, Jul. 2016, doi: 10.1007/s12555-015-0089-9.

[8] H. Kaufman, I. Barkana, and K. Sobel, "Direct Adaptive Control Algorithms: Theory and Applications," in *Direct Adaptive Control Algorithms: Theory and Applications*, 1st ed. New York, NY, USA: Springer-Verlag, 1994, ch. 3, pp. 164–169.

[9] I. Barkana, "Gain conditions and convergence of simple adaptive control," *Int. J. Adaptive Control Signal Process.*, vol. 19, no. 1, pp. 13–40, 2004, doi: 10.1002/acs.830.

[10] S. Ulrich, A. Saenz-Otero, and I. Barkana, "Passivity-based adaptive control of robotic spacecraft for proximity operations under uncertainties," *J. Guid., Control, Dyn.*, vol. 39, no. 6, pp. 1441–1450, 2016, doi: 10.2514/1.G001491.

[11] I. Barkana, "Simple adaptive control: The optimal model reference-short tutorial," in *Proc. 11th IFAC Int. Workshop Adapt. Learn. Control Signal Process.*, Caen, France, Jul. 2013, vol. 46, no. 11, pp. 396–407.

[12] I. Rusnak, J. Weiss, and I. Barkana, "Improving the performance of existing missile autopilot using simple adaptive control," *Int. J. Adaptive Control Signal Process.*, vol. 28, no. 7, pp. 732–749, 2014, doi: 10.1002/acs.2457.

[13] S. Ulrich and J. deLafontaine, "Autonomous atmospheric entry on mars: Performance improvement using a novel adaptive control algorithm," *J. Astronautical Sci.*, vol. 55, no. 4, pp. 431–449, 2007, doi: 10.1007/BF03256534.

[14] T. Takagi, M. Ito, and I. Mizumoto, "Parameter optimization of simple adaptive control via differential evolution," in *Proc. 6th Int. Symp. Adv. Control Ind. Process.*, 2017, pp. 318–323, doi: 10.1109/ADCONIP.2017.7983800.

[15] N. Prabhakar, A. Painter, R. Prazenica, and M. Balas, "Trajectory-driven adaptive control of autonomous unmanned aerial vehicles with disturbance accommodation," *J. Guid., Control, Dyn.*, vol. 41, no. 9, pp. 1976–1989, 2018, doi: 10.2514/1.G003341.

[16] I. BarKana, "Parallel feedforward and simplified adaptive control," *Int. J. Adaptive Control Signal Process.*, vol. 1, no. 2, pp. 95–109, 1987, doi: 10.1002/acs.4480010202.

[17] H. Shibata, T. Fujinaka, and Y. Sun, "A discrete-time algorithm for simple adaptive control," *IFAC Proc. Vol.*, vol. 30, no. 3, pp. 349–354, 1997, doi: 10.1016/s1474-6670(17)44520-4.

[18] M. J. Balas and S. A. Frost, "Sensor blending for direct adaptive control of non-minimum phase linear infinite-dimensional systems in Hilbert space," in *Proc. Amer. Control Conf.*, Seattle, WA, USA, May 2017, pp. 474–480, doi: 10.23919/ACC.2017.7962998.

[19] M. N. Ab Wahab, S. Nefti-Meziani, and A. Atyabi, "A comprehensive review of swarm optimization algorithms," *PLoS One*, vol. 10, no. 5, 2015, Art. no. e0122827, doi: 10.1371/journal.pone.0122827.

[20] S. Ulrich, D. L. Hayhurst, A. Saenz-Otero, D. W. Miller, and I. Barkana, "Simple adaptive control for spacecraft proximity operations," in *Proc. AIAA Guid., Navigation, Control Conf.*, National Harbor, MD, USA, Jan. 2014, pp. 1288–1310, doi: 10.2514/6.2014-1288.

[21] A. Predmyrskyy and S. Ulrich, "Swarm optimized simple adaptive controller for spacecraft proximity operations trajectory tracking," *Int. Federation Autom. Control 2020*, vol. 53, no. 2, pp. 3785–3790, Berlin, Germany, Dec. 2020, doi: 10.1016/j.ifacol.2020.12.2068.

[22] K. Schittkowski, "NLPQL: A FORTRAN subroutine solving constrained nonlinear programming problems," *Ann. Operations Res.*, vol. 5, no. 6, pp. 485–500, 1985, doi: 10.1007/BF02022087.

[23] P. Lu and X. Liu, "Autonomous trajectory planning for rendezvous and proximity operations by conic optimization," *J. Guid., Control, Dyn.*, vol. 36, no. 2, pp. 375–389, 2013, doi: 10.2514/1.58436.

Andriy Predmyrskyy was born in Kiev, Kyivska Oblast, Ukraine, in 1996. He received the B.Eng. and M.A.Sc. degrees in aerospace engineering from Carleton University, Ottawa, Ottawa, ON, Canada, in 2019 and 2021, respectively. He has been a Research Assistant with Spacecraft Robotics and Control Laboratory, Carleton University, since May 2019. From May 2017 to August 2018, he took part in experimental research with the Simulations, Modelling, and Development group, National Research Council's Flight Research Laboratory, authoring two reports on control of experimental aircraft. From May to August 2019, he was a Control Engineer with Kraken Robotics, modeling, simulating, and controlling their Katfish and THUNDERFISH AUVs. His research interests include control systems theory, robust and optimal control, adaptive control, nonlinear system dynamics, spacecraft trajectory tracking, spacecraft formation flying, probabilistic guidance and path planning, optimization, spacecraft autonomy, and autonomous system design.

Mr. Predmyrskyy was the recipient of an Alexander Graham Bell Canada Graduate Scholarship from the National Sciences and Engineering Research Council of Canada.

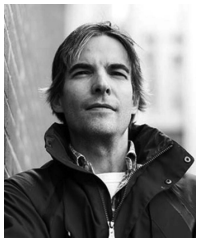

Steve Ulrich (Senior Member, IEEE) received the B.Eng. and M.A.Sc. degrees in electrical engineering from the Université de Sherbrooke, Sherbrooke, QC, Canada, in 2004 and 2006, respectively, and the Ph.D. degree in aerospace engineering from Carleton University, Ottawa, ON, Canada, in 2012.

He is currently an Associate Professor with the Department of Mechanical and Aerospace Engineering, Carleton University. From 2006 to 2008, he was Spacecraft GN&C Research Engineer with NGC Aerospace Ltd. In 2013, he was a Postdoctoral Associate with the Space Systems Laboratory, Massachusetts Institute of Technology, where he contributed to the design and development of GN&C techniques for close-proximity operations using the SPHERES facility aboard the International Space Station. His research interests include path planning, adaptive and learning systems, robotics, and computer vision with applications to spacecraft formation flying and proximity operations.

Dr. Ulrich was the recipient of a Carleton's Research Achievement Award in 2020, a Ministry of Research, Innovation and Science's Early Researcher Award in 2019, and the Best Paper Award at the 2017 International Conference on Control, Dynamic Systems, and Robotics. For his Ph.D. work on adaptive control applied to space robotics, he was awarded a Senate Medal and the E.Y. and J.W. Research Award in Mechanical/Aerospace Engineering. He is a Senior Member of the American Astronautical society (AAS) and American Institute of Aeronautics and Astronautics, and a member of the IFAC Adaptive and Learning Systems Technical Committee. He is currently serving as an Associate Editor for The *Journal of the Astronautical Sciences*.